Dalton Transactions

ARTICLE

Synthesis, Crystal Structure and Spectroscopic Properties of a Novel Yttrium(III) Fluoride Dimolybdate(VI): YFMo$_2$O$_7$

Ingo Hartenbach[a,*], Henning A. Höppe[b], Karolina Kazmierczak[b], and Thomas Schleid[a]

Abstract. Thermal treatment of a mixture of Y$_2$O$_3$, YF$_3$ and MoO$_3$ in a 1 : 1 : 6 molar ratio at 850 °C in evacuated silica ampoules yielded in colorless, platelet-shaped single crystals of YFMo$_2$O$_7$. SiO$_2$ was dissolved from the ampoule wall in small amounts, but could be removed from the crude product by treatment with hydrofluoric acid (20 %). The title compound crystallizes monoclinically in space group $P2/c$ with two formula units per unit cell with the dimensions a = 4.2609(2), b = 6.5644(4), c = 11.3523(7) Å, and β = 90.511(2)°. Its crystal structure contains crystallographically unique Y^{3+} cations in a pentagonal bipyramidal environment consisting of two F$^-$ anions in apical and five O^{2-} anions in equatorial position. These polyhedra are connected to $\frac{1}{\infty}\{[YF_{2/2}^y O_{5/1}^t]^{8-}\}$ chains along [100] by sharing common F$^-$ vertices. The likewise crystallographically unique Mo^{6+} cations exhibit a coordination number of five and reside in the centers of distorted square pyramids built up by oxide anions. These entities are fused to chains along [001] by sharing common edges and vertices according to $\frac{1}{\infty}\{[MoO_{2/2}^s O_{1/2}^y O_{2/1}^t]^-\}$. Taking a sixth oxygen ligand further away from the Mo^{6+} cations into account, the aforementioned chains assemble to corrugated $\frac{2}{\infty}\{[MoO_{2/2}^s O_{3/2}^y O_{1/1}^t]^-\}$ layers perpendicular to [010] with the $\frac{1}{\infty}\{[YF_{2/2}^y O_{5/1}^t]^{8-}\}$ chains situated between these sheets. Since Y^{3+} represents a *non*-luminescent rare-earth metal(III) cation, YFMo$_2$O$_7$ is a suitable host material for doping with luminescent-active lanthanoid(III) cations, such as Eu^{3+}.

Introduction

The quest for energy efficient materials became the major effort of scientific research for more than the last decade. This includes the search for compounds, which display the ability to convert invisible electromagnetic radiation into visible light. In the past, oxidomolybdates(VI) of yttrium (*e. g.* Y$_2$[MoO$_4$]$_3$ and Y$_2$[MoO$_4$]$_2$[Mo$_2$O$_7$])[1] and their fluoride derivatives (*e. g.* YF[MoO$_4$])[2] have proven to be suitable host materials for luminescence applications. The most interesting fact about these classes of compounds is the ability of the oxidomolybdate(VI) groups to harvest light from the UV region of the spectral band utilizing their ligand-to-metal charge transfer (LMCT) process and subsequently transfer this energy to a luminescent-active cation such as Eu^{3+} or Tb^{3+}, causing these to emit visible light. If the structure contains only discrete tetrahedral *ortho*-oxidomolybdate(VI) entities [MoO$_4$]$^{2-}$, the LMCT energy is located at about 290 nm.[3] By altering the size of these units to dimolybdate(VI) pyroanions[1] [Mo$_2$O$_7$]$^{2-}$ or higher aggregated entities, it is possible to shift this wavelength towards an area of lower energy. Besides the aforementioned

O^{2-}→Mo^{6+} LMCT, the O^{2-}→Eu^{3+} charge transfer process has to be taken into account as well, although the latter strongly depends on the coordination environment of the europium(III) cations in the actual crystal structure. The title compound YFMo$_2$O$_7$ represents the first fluoride-derivatized yttrium(III) oxidomolybdate(VI) with an extended molybdate substructure, in which the coordination spheres of the central molybdenum(VI) cations are enlarged and no isolated [Mo$_2$O$_7$]$^{2-}$ pyroanions are present. This increase of the coordination number for Mo^{6+} is observed for quite a few compounds, *e. g.* C. N. = 5, represented by isolated [MoO$_5$]$^{4-}$ anions in Ce$_2$[MoO$_4$][MoO$_5$],[4] or C. N. = 6, found as edge-sharing [MoO$_6$]$^{6-}$ octahedra in *Keggin*-type anions as in H$_3$[PMo$_{12}$O$_{40}$] · 6 H$_2$O,[5] for example.

Experimental

Synthesis

YFMo$_2$O$_7$ was obtained from a mixture of yttrium sesquioxide (Y$_2$O$_3$: 99.9 %; ChemPur, Karlsruhe, Germany), yttrium

trifluoride (YF$_3$: 99.9 %; ChemPur, Karlsruhe, Germany), and molybdenum trioxide (MoO$_3$: *p. a.*; Merck, Darmstadt, Germany) in a 1 : 1 : 6 molar ratio, which was tempered at 850 °C for six days in evacuated silica ampoules according to equation (1):

(1) $\quad$ Y$_2$O$_3$ + YF$_3$ + 6 MoO$_3$ $\rightarrow$ 3 YFMo$_2$O$_7$.
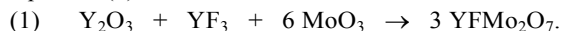
From this reaction colorless, transparent, platelet-shaped crystals of the title compound were obtained, which remained stable in air and water, while a shorter reaction time only yields a microcrystalline crude product. The use of fluoride anions from YF$_3$ resulted in a minor impurity of SiO$_2$ in the crude product, which was dissolved from the ampoule wall and recrystallized to *α-cristobalite*-type silicon dioxide. This undesired by-product could be removed by treatment of the reaction products with an aqueous solution of hydrofluoric acid (20 %), which transformed the SiO$_2$ component to soluble [SiF$_6$]$^{2-}$, SiF$_4$ or silicon oxide fluorides which are volatile at room temperature. The remaining product was unharmed by this procedure and could be identified as single-phase YFMo$_2$O$_7$ according to X-ray powder diffraction (Fig. 1). In order to synthesize Eu^{3+}-doped samples, about 2 % of the yttrium sesquioxide was replaced by europium sesquioxide (Eu$_2$O$_3$: 99.9 %; ChemPur, Karlsruhe, Germany) in the educt mixture, while the reaction conditions as well as the rinsing treatment of the crude product remained the same as for the undoped compound. Synthesis routes which are more energy efficient, such as solvochemical routes, have proven to be unsuccessful, so far.

X-ray crystallography

The X-ray powder patterns were measured on a Stoe STADI P diffractometer with a position-sensitive detector using germanium-monochromatized Cu-Kα radiation (wavelength: λ = 1.5406 Å, step size 0.1°, irradiation time 60 s). The refinement of the powder diffractogram (Fig. 1) was performed with the help of the program FULLPROF (Version 2K^2) implemented in the WINPLOTR program suite.[6] Deviations of intensities within the powder diffractogram are due to texture effects of the mostly platelet shaped microcrystals.
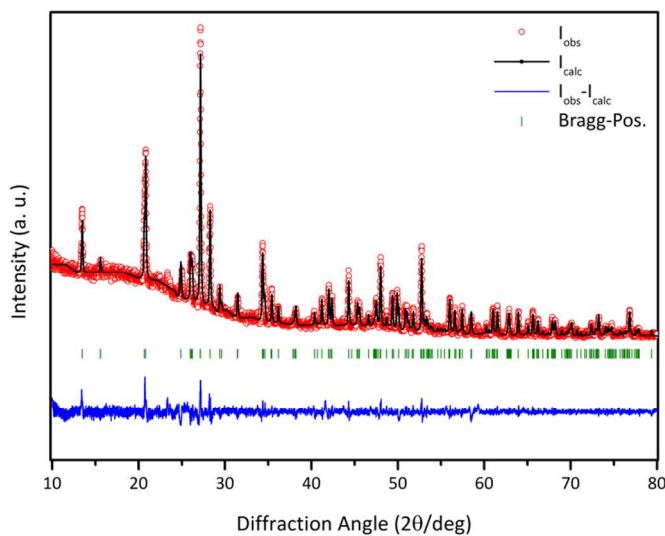

Figure 1. X-ray powder diffractogram of single phase YFMo$_2$O$_7$

Intensity data sets for single crystals of YFMo$_2$O$_7$ were collected on a Nonius Kappa-CCD diffractometer using graphite-monochromatized Mo-Kα radiation (wavelength: λ = 0.7107 Å, φ- and ω-scans, irradiation time: 20 s/deg). Numerical absorption correction was carried out with the help of the program HABITUS[7], and structure solution and refinement were performed with the program suite SHELX-97.[8] Details of the data collection and the structure refinement[9] are summarized in Table 1, atomic positions and coefficients of the isotropic thermal displacement parameters[10] are shown in Table 2, and motifs of mutual adjunction[11] as well as interatomic distances are given in Table 3. Further details of the crystal structure investigation are available from the Fachinformationszentrum (FIZ) Karlsruhe, D-76344 Eggenstein-Leopoldshafen, Germany (Fax: +49(0)7247-808-444; e-mail: crysdata@fiz-karlsruhe.de), on quoting the depository number CSD-427022 for YFMo$_2$O$_7$.

Table 1. Crystallographic data for YFMo$_2$O$_7$.

Empirical formula	YFMo$_2$O$_7$
Crystal system; space group formula units	monoclinic; *P*2/*c* (no. 13) $Z = 2$
Lattice constants, *a* / Å	4.2609(2)
b / Å	6.5644(4)
c / Å	11.3523(7)
β / deg	90.511(2)
Calculated density, D_x / g · cm^{-3}	4.307
Molar volume, V_m / cm^3 · mol^{-1}	95.605
F(000); absorption coefficient, μ / mm^{-1}	376; 12.963
Index range ($\pm h$ / $\pm k$ / $\pm l$); theta range ($\theta_{min} - \theta_{max}$)	5 / 8 / 15; 3.10 − 28.25
Data corrections	background, polarization and Lorentz factors; numerical absorption correction with the program HABITUS[7]
Collected / unique reflections / free parameters	7716 / 797 / 54
R$_{int}$ / R$_\sigma$	0.087 / 0.031
R$_1$ for / # reflections with |F$_o$| $\geq$ 4σ(F$_o$)	0.021 / 795
R$_1$ / wR$_2$ for all reflections	0.021 / 0.053
Goodness of fit (GooF)	1.088
Extinction coefficient, *g*	0.071(3)
Residual electron density, ρ / e$^-$ · 10^{-6} pm^{-3}	max.: 0.79, min.: –0.82

Table 2. Atomic coordinates and equivalent isotropic displacement factors $U_{eq}^{a)}$ for $YFMo_2O_7$.

Atom	Wyckoff position	x / a	y / b	z / c	U_{eq} / Å²
Y	2e	0	0.79522(8)	¼	0.0083(2)
F	2f	½	0.8035(6)	¼	0.0280(9)
Mo	4g	0.09830(7)	0.33053(5)	0.09409(3)	0.0097(1)
O1	4g	0.4972(7)	0.3428(4)	0.0972(3)	0.0181(6)
O2	4g	0.0164(7)	0.0778(4)	0.1271(2)	0.0170(6)
O3	4g	0.0026(7)	0.6498(4)	0.0663(2)	0.0135(5)
O4	2e	0	0.4389(6)	¼	0.0121(7)

$^{a)}$ U_{eq} is defined as ⅓ of the trace of the orthogonalized U_{ij} tensor.[10]

Table 3. Motifs of mutual adjunction[11] and selected interatomic distances (in Å) for $YFMo_2O_7$.

	F	O1	O2	O3	O4	C. N.
Y	2 / 2 2.131(2)	0 / 0	2 / 1 2.323(2)	2 / 1 2.294(3)	1 / 1 2.339(4)	7
Mo	0 / 0	1+1 / 1+1 1.701(3) *2.563(3)*	1 / 1 1.737(3)	2 / 2 1.811(3) 2.158(3)	1 / 2 1.956(2)	5 + 1
C. N.	2	1 + 1	2	3	3	

IR and *Raman* spectroscopy

The infrared spectrum of $YFMo_2O_7$ was recorded on a Thermo Scientific Nicolet iS5 spectrometer equipped with an ATR unit using a diamond crystal measuring the reflection of the powdered sample. *Raman* spectroscopy was performed with the help of a Thermo Scientific DXR SmartRaman 780 spectrometer using a green excitation laser (wavelength: λ = 780 nm) for irradiation of the compressed powder sample.

UV-Vis and luminescence spectroscopy

Diffuse reflectance spectra were collected on a J & M TIDAS UV-Vis-NIR spectrophotometer equipped with a reflectance measuring geometry. A barium sulfate standard was used as white reference and the *Kubelka-Munk* function was applied to obtain band-gap information.[12] The position of the onset point of the band gap was determined by the intersection of the linear fit at the steepest slope with the linear baseline fit of the spectrum. The maximum of the band gap was determined by the position of the inflection point in the steepest slope within the spectrum. Solid-state excitation and emission spectra were recorded at room temperature using a Horiba FluoroMax-4 fluorescence spectrometer equipped with a xenon discharge lamp scanning a range from 200 to 800 nm. Electronic

transitions were assigned according to the energy-level diagrams of trivalent europium cations.[13]

Results and Discussion

Crystal structure

$YFMo_2O_7$ crystallizes monoclinically in space group $P2/c$ (a = 4.2609(2), b = 6.5644(4), c = 11.3523(7) Å, β = 90.511(2)°) with two formula units per unit cell. The crystallographically unique Y^{3+} cations reside on *Wyckoff* position 2e (symmetry: 2) with pentagonal bipyramids built up by two F^- anions representing the apical vertices and five O^{2-} ligands in the equatorial plane as coordination environment (Fig. 2, *left*). These $[YF_2O_5]^{9-}$ polyhedra share common fluoride vertices to form $_\infty^1\{[YF_{2/2}O_{5/1}]^{8-}\}$ chains along [100] (Fig. 2, *right*).
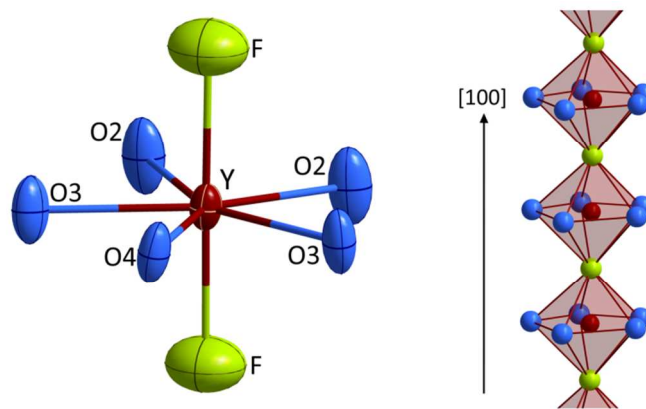

Figure 2. Coordination environment of the Y^{3+} cations (*left*) and $_\infty^1\{[YF_{2/2}O_{5/1}]^{8-}\}$ chains along [100], which form by sharing the fluoride vertices of pentagonal $[YF_2O_5]^{9-}$ bipyramids in the crystal structure of $YFMo_2O_7$ (ellipsoid representation at 95 % probability).

Although the distances between Y^{3+} and F^- are unusually short with a value of 2.131(3) Å (2×), there are quite a few compounds, *e. g.* Cs_2KYF_6 exhibiting the same short $Y^{3+}-F^-$ distances of 2.13 Å.[14] The distances between yttrium and oxygen range between 2.29 and 2.34 Å, which is also found in most compounds containing yttrium and oxygen, including in *bixbyite*-type yttrium sesquioxide (Y_2O_3) itself ($d(Y^{3+}-O^{2-})$ = 2.25 – 2.35 Å).[15] The crystal structure exhibits crystallographically unique Mo^{6+} cations, located at the general *Wyckoff* position 4g, which are surrounded by five oxygen atoms in the shape of a distorted square pyramid (Fig. 3, *left*). The molybdenum-oxygen distances cover a broad range between 1.70 and 2.16 Å. While the shorter distances of 1.70 and 1.74 Å are typical for terminal $Mo^{6+}-O^{2-}$ contacts as found *e. g.* in $K_2[MoO_4]$, which contains isolated *ortho*-oxidomolybdate(VI) tetrahedra ($d(Mo^{6+}-O^{2-})$ = 1.74 – 1.78 Å)[16], the larger ones of 1.87 – 2.16 Å appear common for those representing connective vertices or even parts of linking edges, just like in molybdenum trioxide (MoO_3) itself ($d(Mo^{6+}-O^{2-})$ = 1.87 – 2.45 Å).[17] The $[MoO_5]^{4-}$ pyramids link together to form

$\frac{1}{\infty}\{[MoO_{2/2}^e\,O_{1/2}^v\,O_{2/1}^t]^-\}$ (e = edge, v = vertex, t = terminal) chains along [001] via common oxide vertices and edges (Fig. 3, *right*).
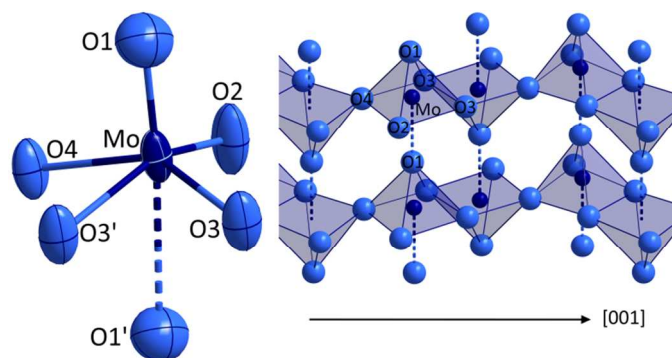

Figure 3. Coordination environment of the Mo^{6+} cations (*left,* ellipsoid representation at 95 % probability), including a sixth fairly long contact (*dashed line*), and $\frac{1}{\infty}\{[MoO_{2/2}^e\,O_{1/2}^v\,O_{2/1}^t]^-\}$ chains along [001] (*right*), which are interconnected by the aforementioned extra contact to corrugated $\frac{2}{\infty}\{[MoO_{2/2}^e\,O_{3/2}^v\,O_{1/1}^t]^-\}$ layers parallel to the (010) plane.

The terminal (O1)$^{2-}$ anions display a second, long-distance contact of 2.56 Å to the Mo^{6+} cations increasing their coordination number to 5 + *1* and expanding the coordination polyhedra to highly distorted octahedra with eccentrically coordinated Mo^{6+} cations (Fig. 3, *left*). The aforementioned $\frac{1}{\infty}\{[MoO_{2/2}^e\,O_{1/2}^v\,O_{2/1}^t]^-\}$ strands are subsequently connected to each other, forming corrugated $\frac{2}{\infty}\{[MoO_{2/2}^e\,O_{3/2}^v\,O_{1/1}^t]^-\}$ layers perpendicular to the [010] direction (Fig. 3, *right*). According to ECoN calculations (**E**ffective **Co**ordination **N**umbers)[18] the most distant attractive contact (2.56 Å) between Mo^{6+} and (O1)$^{2-}$ has no contribution to the effective coordination numbers (ECoN) of either atom, however, the description of the structure can be simplified by taking it into consideration anyhow. Therefore, the crystal structure can be described as if being assembled by layers of the composition $\frac{2}{\infty}\{[MoO_{2/2}^e\,O_{3/2}^v\,O_{1/1}^t]^-\}$ spreading out parallel to the (010) plane, between which $\frac{1}{\infty}\{[YF_{2/2}]^{2+}\}$ strands are situated running along [100] (Fig. 4).
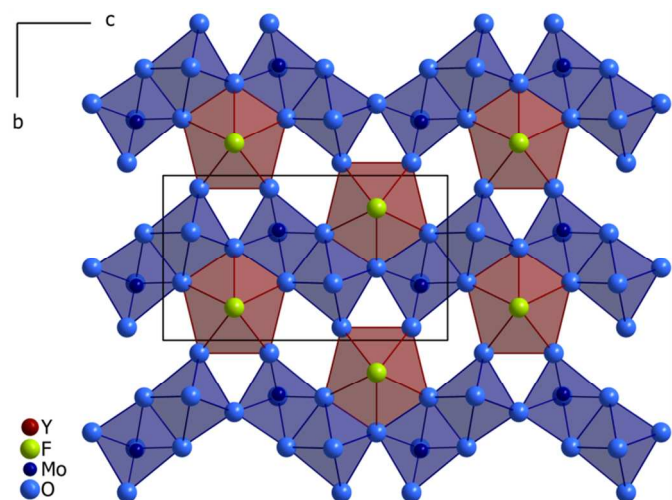

Figure 4. View at the crystal structure of YFMo$_2$O$_7$ along the *a* axis. The structure can be described as being built up by $\frac{2}{\infty}\{[MoO_{2/2}^e\,O_{3/2}^v\,O_{1/1}^t]^-\}$ layers (represented by blue polyhedra) and $\frac{1}{\infty}\{[YF_{2/2}]^{2+}\}$ strands (within the red polyhedra).

The monoclinic angle of almost 90° suggests a strong relationship to the orthorhombic crystal system, however, a structure solution in an orthorhombic supergroup of *P*2/*c* places the Mo^{6+} cations right into the centers of the aforementioned oxygen octahedra. Since the maxima of the electron density in the final structure-refinement cycles remain more than 0.4 Å offset towards one of the (O1)$^{2-}$ vertices (Fig. 5), mirror planes perpendicular to [100] cannot be postulated seriously, hence only monoclinic symmetry is found.

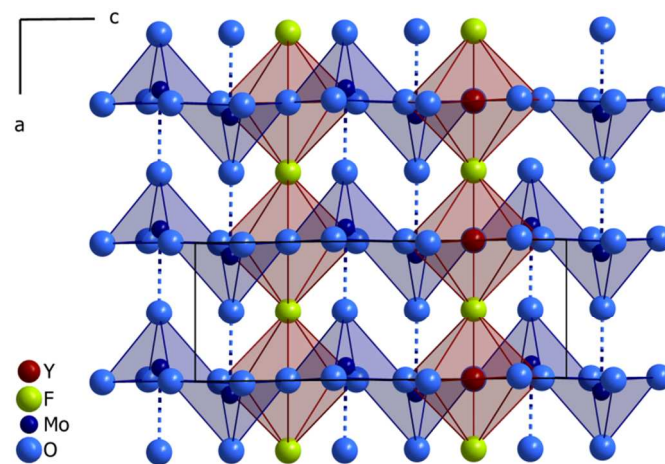**Figure 5.** View at the crystal structure of YFMo$_2$O$_7$ along the *b* axis. While all the atoms are situated more or less on imaginary mirror planes at $x/a = 0$ and $^1/_2$, respectively, the Mo^{6+} cations reside about 0.4 Å offset.

IR and *Raman* spectroscopy

The distorted square oxidomolybdate(VI) pyramids [MoO$_5$]$^{4-}$ within the $\frac{2}{\infty}\{[MoO_{2/2}^e\,O_{3/2}^v\,O_{1/1}^t]^-\}$ layers display merely symmetry 1 (C$_1$), offering the usual range for stretching vibrations of these pyramidal entities situated in the same area as found for tetrahedral [MoO$_4$]$^{2-}$ anions, *i. e.* between 800 and 1000 wavenumbers.[19] In the IR spectrum (Fig. 6, *top*) two wide peaks, which both appear to be superimposed peaks each, are found between 840 and 980 wavenumbers, typically assignable to Mo–O stretching vibrations with the symmetric one at the highest energy. According to *Busca*[19] the Mo–O–Mo stretching vibrations of the vertex-linked regions within the oxidomolybdate(VI) layers can be detected at energies lower than 800 wavenumbers, which coincides well with another very wide band at about 760 cm^{-1} seen in the IR spectrum. In the *Raman* spectrum (Fig. 6, *bottom*) two very strong peaks at 945 and 901 cm^{-1}, respectively, are found, which can again be assigned to symmetric and asymmetric stretching vibrations, while the very weak ones between 700 and 800 cm^{-1}, presumably also attributing to Mo–O and Mo–O–Mo stretching

modes. The deformation vibrations of the oxidomolybdate(VI) units are expected well below 400 cm^{-1}, which cannot be detected in the IR spectrum due to device restrictions. These modes become visible in the *Raman* spectrum, however, in the supposed range below 400 cm^{-1}, but since Y–F and Y–O stretching modes are also present there, an explicit assignment of the peaks is not possible.
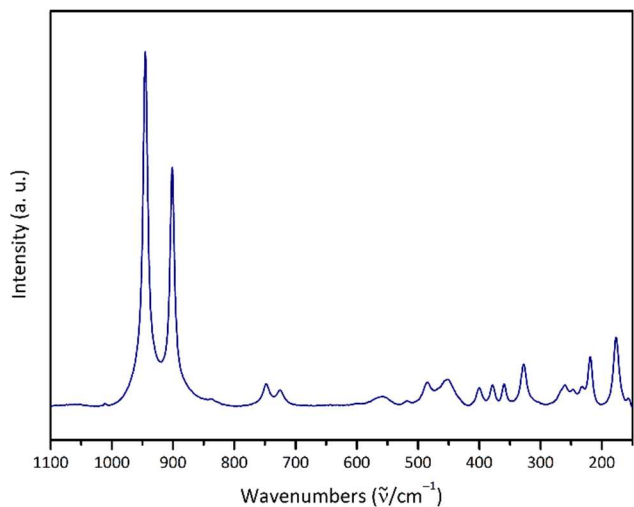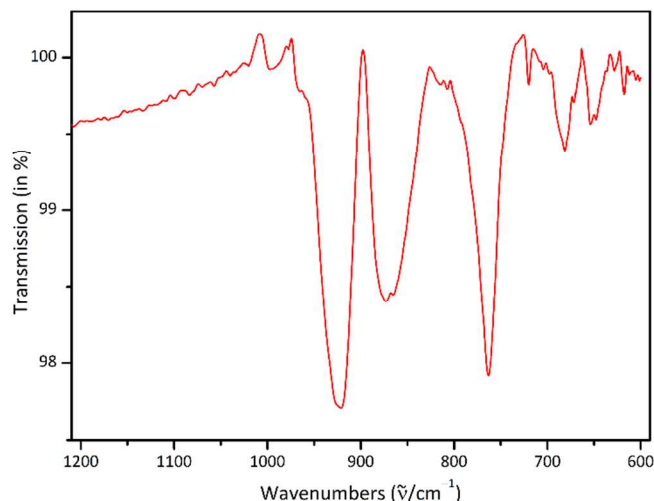

Figure 6. Infrared (*top*) and *Raman* spectrum (*bottom*) of $YFMo_2O_7$.

UV-Vis and photoluminescence spectroscopy

Yttrium(III) oxidomolybdates(VI) as well as their fluoride derivatives have already proven to be suitable host materials for luminescence-active lanthanoid(III) cations, such as Eu^{3+}.[1, 2] Doping experiments with the title compound have also been successful in yielding $YFMo_2O_7:Eu^{3+}$, which shows a bright red luminescence under UV irradiation (λ_{exc} = 366 nm). In the emission spectrum the strongest peak at 612 nm (*red curve* in Fig. 7) is assigned to the $^5D_0 \rightarrow {}^7F_2$ electric dipole transition, because the Eu^{3+} cations, which substitute Y^{3+} at their crystallographically unique positions, are not located on an inversion center in the crystal structure. Hence, the $^5D_0 \rightarrow {}^7F_1$ magnetic dipole transition is also visible at 591 nm, displaying a minor contribution to the overall luminescence intensity.
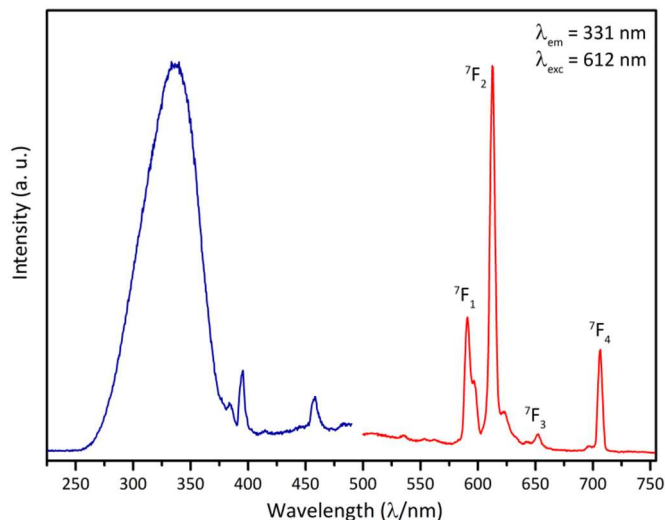

Figure 7. Excitation (*blue*) and emission spectrum (*red*) of $YFMo_2O_7:Eu^{3+}$.

The excitation spectrum (*blue curve* in Fig. 7) shows rather sharp signals at 393 and 464 nm, which are assigned to f–f transitions within the electronic valence shell of the Eu^{3+} cations. In such oxide-based compounds the top of the valence band is usually dominated by oxygen p states, while the bottom of the conduction band can be assigned to d states of the highly oxidized transition metal atom, providing the possibility of $O^{2-} \rightarrow M^{n+}$ charge transfer (CT) transitions.[20] Accordingly, a broad band with a maximum at 325 nm is visible, attributed to the $O^{2-} \rightarrow Mo^{6+}$ CT process in the oxidomolybdate(VI) partial structure as well as to the well-known $O^{2-} \rightarrow Eu^{3+}$ CT transition. In the case of materials consisting of *ortho*-oxidomolybdate(VI) tetrahedra $[MoO_4]^{2-}$, the maximum of the $O^{2-} \rightarrow Mo^{6+}$ CT process is located at about 290 nm with little influence of the surrounding cationic situation.[21] By enlarging the molybdate units by means of condensation (*e. g.* to $[Mo_2O_7]^{2-}$ anions) or enhancing the coordination number of Mo^{6+} from four to five (or even six) this maximum usually shifts towards regions of lower energy as seen in the spectrum of $YFMo_2O_7:Eu^{3+}$ compared to that of $YF[MoO_4]:Eu^{3+}$, where the maximum of the CT band lies at about 290 nm.[2] Unfortunately, it is not easy to distinguish the part of the $O^{2-} \rightarrow Eu^{3+}$ from the $O^{2-} \rightarrow Mo^{6+}$ CT process in the very wide charge transfer band. However, the position of the maximum can be attributed to the $O^{2-} \rightarrow Mo^{6+}$ CT, since the diffuse reflectance spectra of undoped $YFMo_2O_7$ and its Eu^{3+}-doped derivative are extremely similar (Fig. 8). In both spectra the onset point and the maximum of the optical band gap are found at about the same values (~380 nm for the onset point and ~325 nm for the maximum) for the Eu^{3+}-doped and the undoped material, being in good agreement with the values determined from the excitation spectrum of $YFMo_2O_7:Eu^{3+}$ (Fig. 7, *blue curve*). Furthermore, this similarity

also gives evidence to the statement, that the main influence on the position of the broad charge transfer area in the excitation spectrum is dominated by the $O^{2-} \rightarrow Mo^{6+}$ rather than by the $O^{2-} \rightarrow Eu^{3+}$ CT transition. Thus, it appears that shifting this area towards the visible range of the electromagnetic spectrum is indeed possible by enlarging the oxidomolybdate units, either by condensation of tetrahedral $[MoO_4]^{2-}$ anions or by increasing the coordination number of the central Mo^{6+} cations.
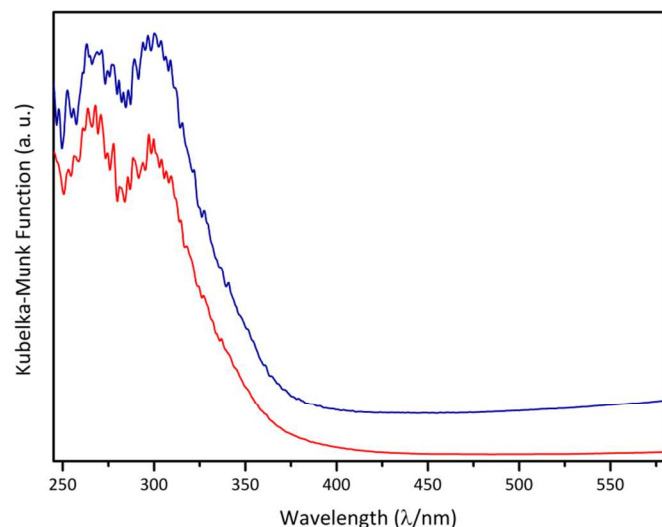
Figure 8. Comparison of the diffuse UV-Vis reflectance spectra of $YFMo_2O_7$ (*blue curve*) with the Eu^{3+}-doped material (*red curve*).

Conclusions

The novel yttrium fluoride dimolybdate $YFMo_2O_7$ and its Eu^{3+}-doped derivative can be synthesized as phase-pure samples by solid-state methods. The crystal structure does not consist of pyroanionic dimolybdate units ($[Mo_2O_7]^{2-}$), but of a layer-like arrangement of distorted octahedral $[MoO_{5+1}]^{6-}$ polyhedra, which are fused together via common edges and vertices. Vibrational spectroscopic investigations were performed as well as optical spectroscopy of both the Eu^{3+}-doped and the undoped material. It was possible to give evidence on the shift of the optical band gap (with the $O^{2-} \rightarrow Mo^{6+}$ CT as its main part) towards lower energies being caused by the enlargement of the oxidomolybdate(VI) array.

Acknowledgements

Notes and references

* To whom correspondence should be addressed: Fax: +49(0)711/685-64254, E-mail: hartenbach@iac.uni-stuttgart.de
a Institute for Inorganic Chemistry, University of Stuttgart, Pfaffenwaldring 55, 70569 Stuttgart, Germany.
b Institute for Physics, University of Augsburg, Universitätsstr. 1, 86159 Stuttgart, Germany.

Electronic Supplementary Information (ESI) available: Crystal information file. See DOI: 10.1039/b000000x/

1   S. Laufer, S. Strobel, Th. Schleid, J. Cybinska, A.-V. Mudring, I. Hartenbach, *New J. Chem.*, 2013, **37**, 1919-1926.
2   Th. Schleid, S. Strobel, P. K. Dorhout, P. Nockemann, K. Binnemans, I. Hartenbach, *Inorg. Chem.*, 2008, **47**, 3728-3735.
3   G. Blasse, B. C. Grabmeier, *Luminescent Materials*, Springer-Verlag: Berlin, Heidelberg, 1994.
4   T. Schustereit, Th. Schleid, I. Hartenbach, *Z. Naturforsch.*, 2011, **66 b**, 763-770.
5   C. J. Clark, D. Hall, *Acta Crystallogr.*, 1976, **B 32**, 1545-1547.
6   T. Roisnel, J. Rodriguez-Carvajal, in *Mater. Sci. Forum, Proceedings of the Seventh European Powder Diffraction Conference EPDIC 7* eds.: R. Delhez, E. J. Mittemeijer, Barcelona, 2000, pp. 118-123.
7   W. Herrendorf, H. Bärnighausen, *HABITUS: Program for the Optimization of the Crystal Shape for Numerical Absorption Correction in X-SHAPE (version 1.06, Fa. Stoe, Darmstadt 1999)*, Karlsruhe, Gießen, 1993, 1996.
8   G. M. Sheldrick, *Acta Crystallogr.*, 2008, **A 64**, 112-122.
9   Th. Hahn, A. J. C. Wilson (eds.), *International Tables for Crystallography*, *Vol. C*, 2nd Edition, Kluwer Academic Publishers: Boston, Dordrecht, London, 1992.
10 R. X. Fischer, E. Tillmanns, *Acta Crystallogr.*, 1988, **C 44**, 775-776.
11 (a) R. Hoppe, *Adv. Fluorine Chem.*, 1970, **6**, 387-438; (b) R. Hoppe, *Izv. Jugoslav. Centr. Krist. (Zagreb)*, 1973, **8**, 21-36; (c) R. Hoppe, in *Crystal Structure and Chemical Bonding in Inorganic Chemistry*, eds.: C. J. M. Rooymans, A. Rabenau, Amsterdam, 1975, p. 127.
12 W. W. Wendlandt, H. G. Hecht, *Reflectance Spectroscopy*, Interscience Publishers, New York, 1966.
13 G. H. Dieke *Spectra and Energy Levels of Rare Earth Ions in Crystals*, Interscience Publishers, New York, 1969.
14 A. Vedrine, J. P. Besse, G. Baud, M. Capestan, *Rev. Chim. Miner.*, 1970, **7**, 593-610.
15 M. G. Paton, E. N. Maslen, *Acta Crystallogr.*, 1965, **19**, 307-310.
16 B. M. Gatehouse, P. Leverett, *J. Chem. Soc. A*, 1969, **1969**, 849-854.
17 N. Wooster, *Z. Kristallogr.*, 1931, **80**, 504-512.
18 R. Hoppe, *Z. Kristallogr.*, 1979, **150**, 23-52.
19 G. Busca, *J. Raman Spectrosc.*, 2002, **33**, 348-358.
20 M. Daub, A. J. Lehner, H. A. Höppe, *Dalton Trans.* 2012, **41**, 12121-12128.
21 G. Blasse, *Struct. Bond.*, 1980, **42**, 1-41.
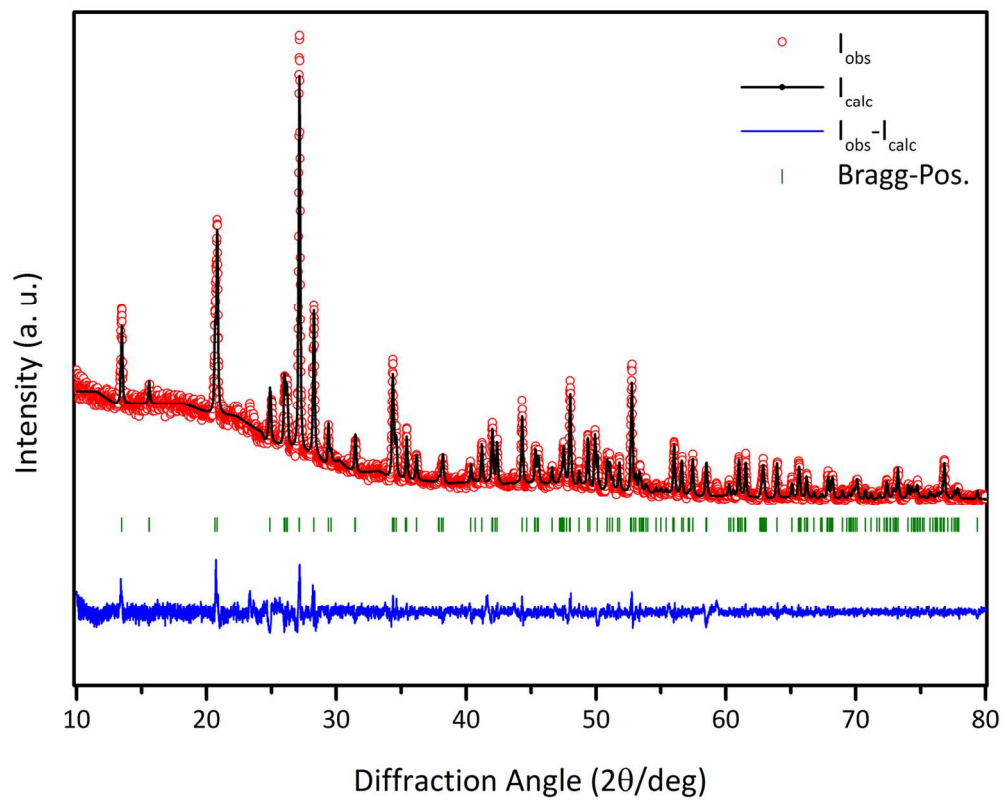
X-ray powder diffractogram of single phase YFMo2O7
137x110mm (300 x 300 DPI)
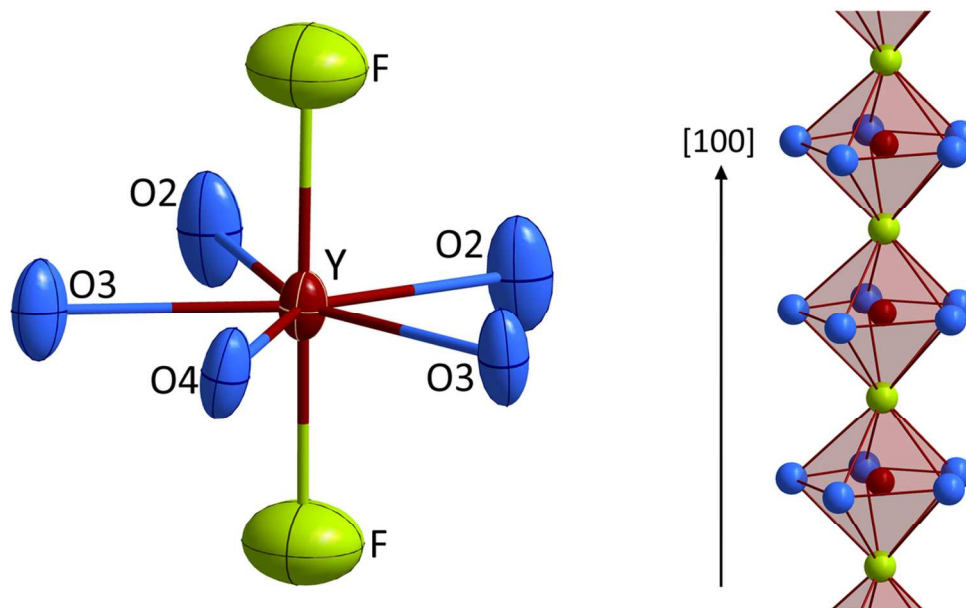
Coordination environment of the Y3+ cations (left) and {[YF O]8−} chains along [100], which form by sharing the fluoride vertices of pentagonal [YF2O5]9− bipyramids in the crystal structure of YFMo2O7 (ellipsoid representation at 95 % probability).
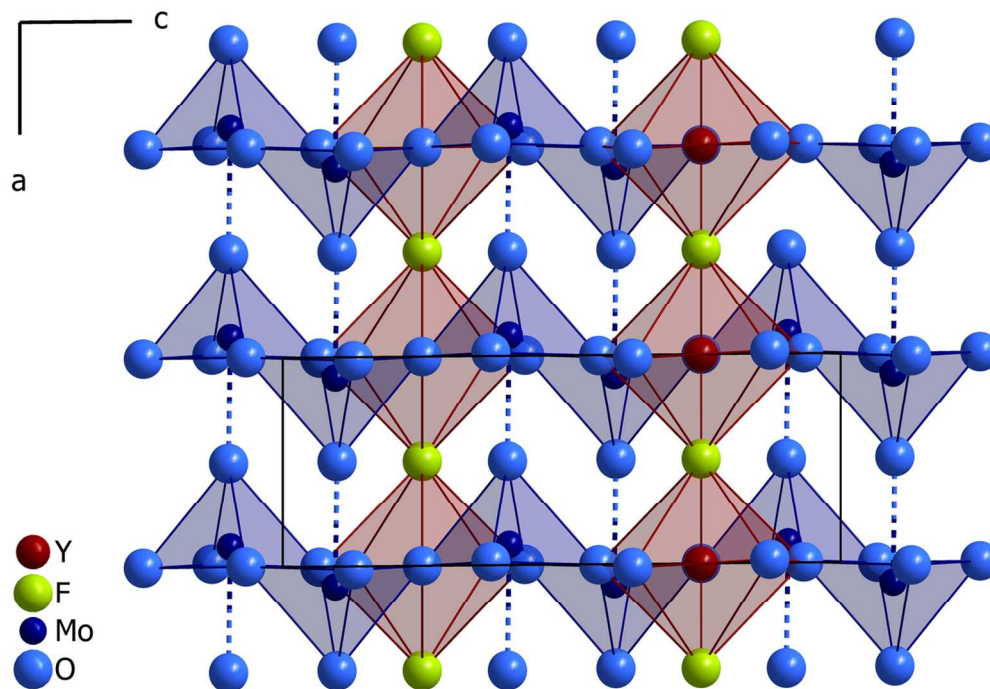107x67mm (300 x 300 DPI)
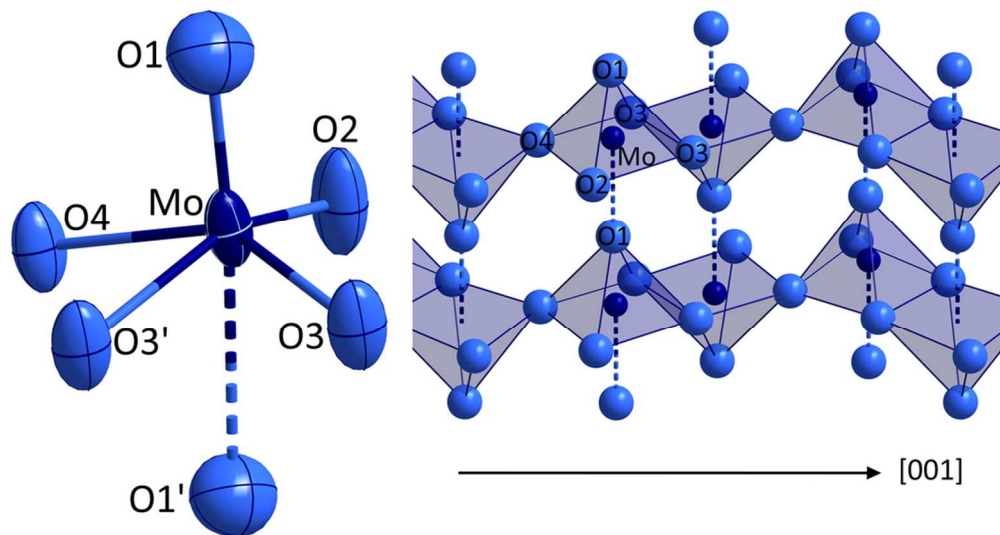
Coordination environment of the Mo6+ cations (left, ellipsoid representation at 95 % probability), including a sixth fairly long contact (dashed line), and {[MoO O O]−} chains along [001] (right), which are interconnected by the aforementioned extra contact to corrugated {[MoO O O]−} layers parallel to the (010) plane.
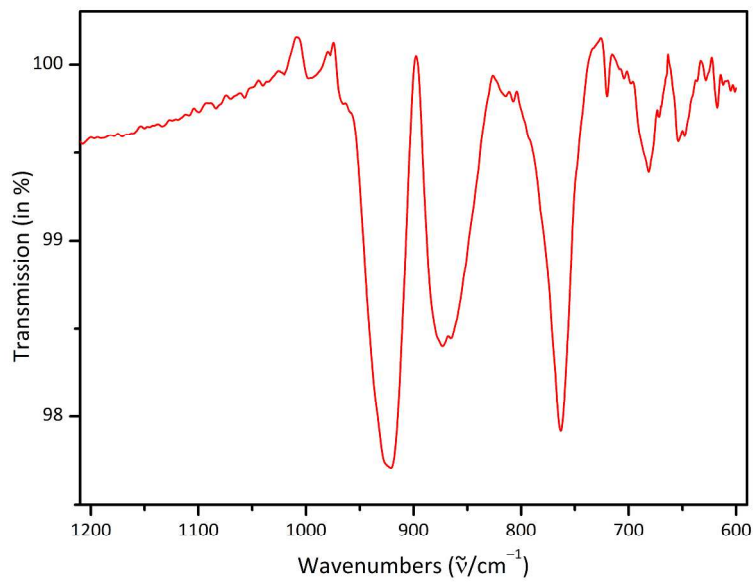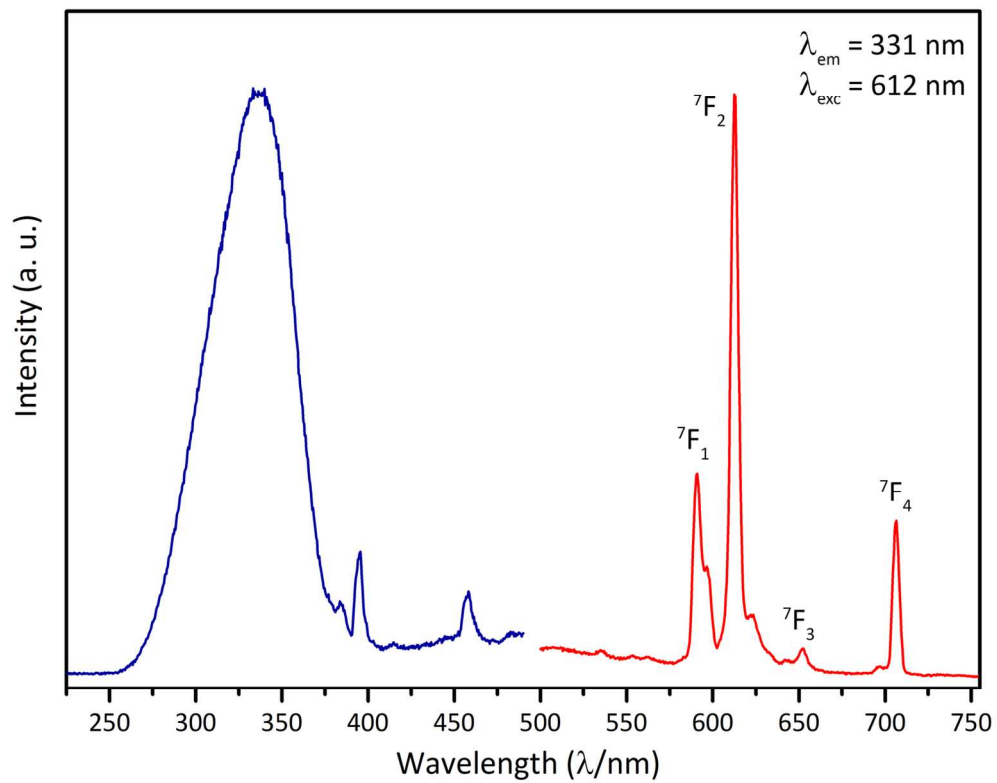90x48mm (300 x 300 DPI)
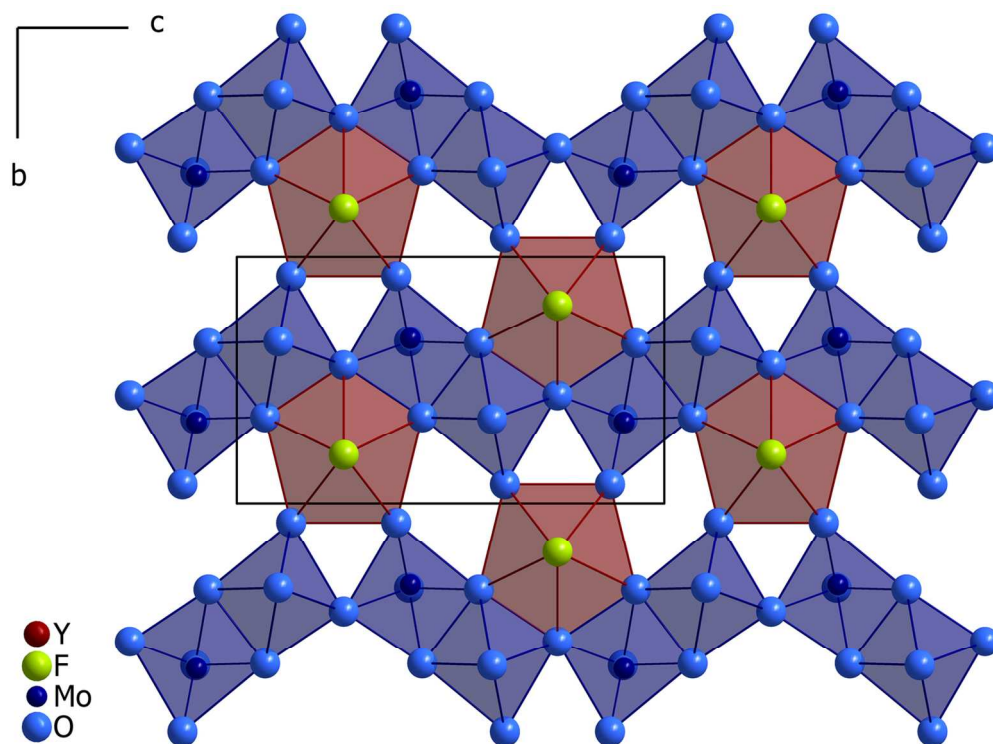
View at the crystal structure of YFMo2O7 along the a axis. The structure can be described as being built up by {[MoO O O]−} layers (represented by blue polyhedra) and {[YF2/2]2+} strands (within the red polyhedra) between them.
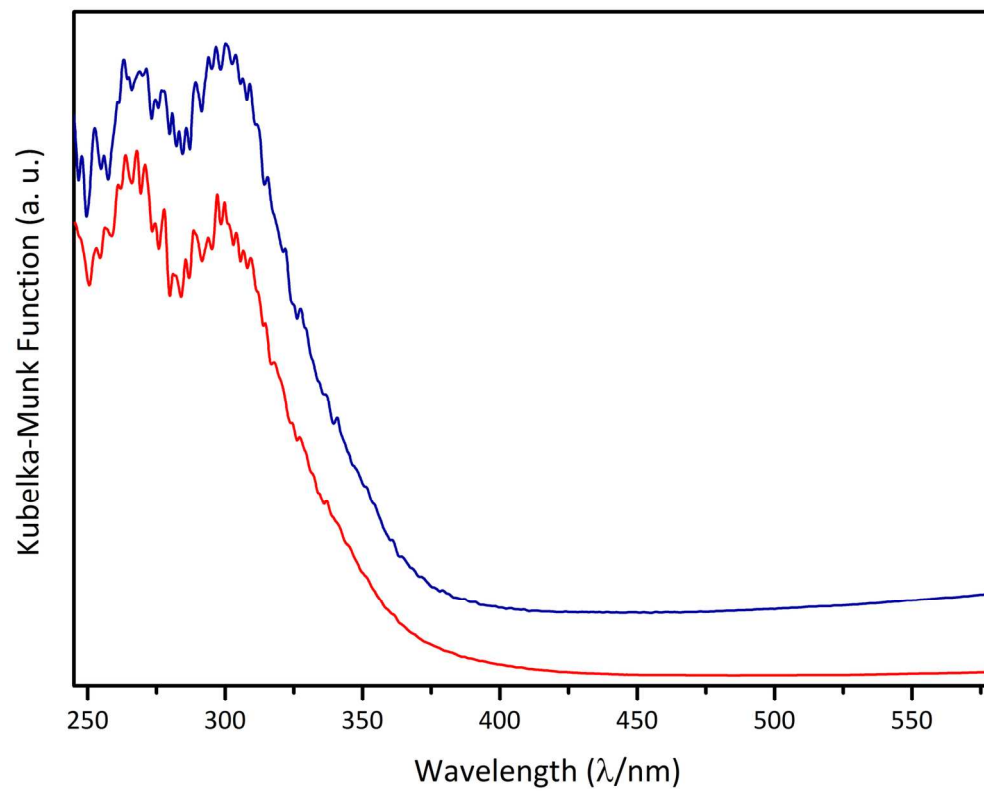127x95mm (300 x 300 DPI)

View at the crystal structure of YFMo2O7 along the b axis. While all the atoms are situated more or less on imaginary mirror planes at x/a = 0 and 1/2, respectively, the Mo6+ cations reside about 40 pm offset.
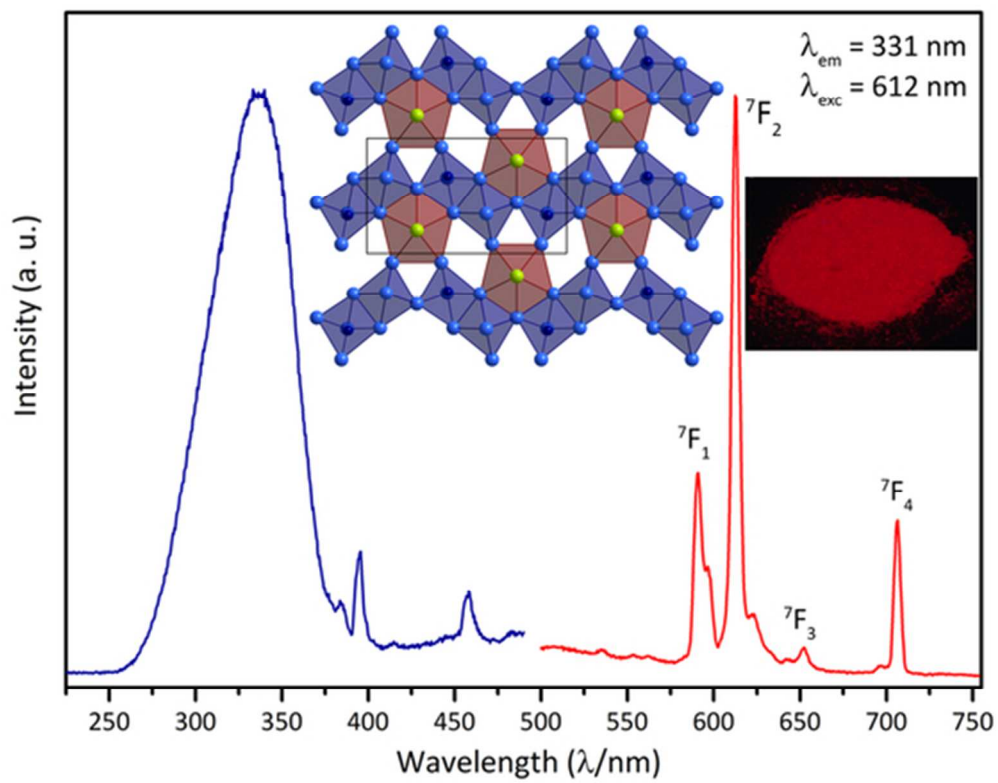118x82mm (300 x 300 DPI)
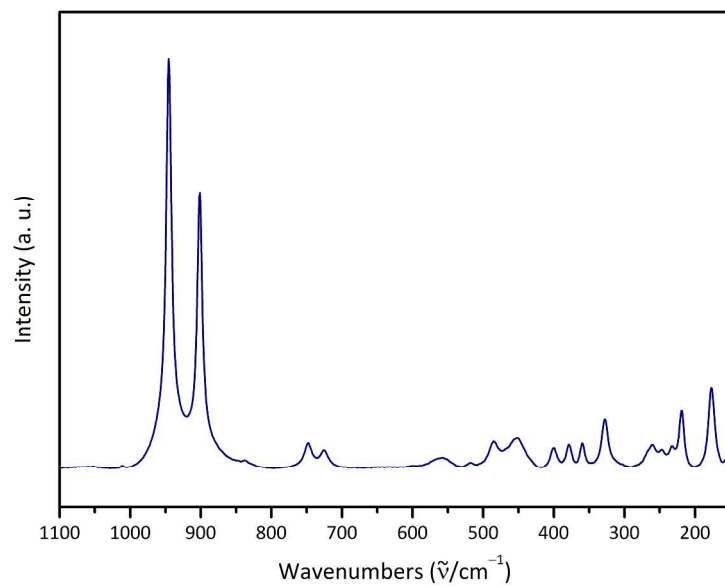
Infrared (top) and Raman spectrum (bottom) of YFMo2O7.
266x416mm (300 x 300 DPI)

Excitation (blue) and emission spectrum (red) of YFMo2O7:Eu3+.
134x106mm (300 x 300 DPI)

Comparison of the diffuse UV-Vis reflectance spectra of YFMo2O7 (blue curve) with the Eu3+-doped material (red curve).
147x117mm (300 x 300 DPI)

47x37mm (300 x 300 DPI)